Journal of
Materials Chemistry C

Materials for optical, magnetic and electronic devices

## Accepted Manuscript

This article can be cited before page numbers have been issued, to do this please use: A. Kumar, E. Bora and T. Debnath, *J. Mater. Chem. C*, 2026, DOI: 10.1039/D6TC00820H.

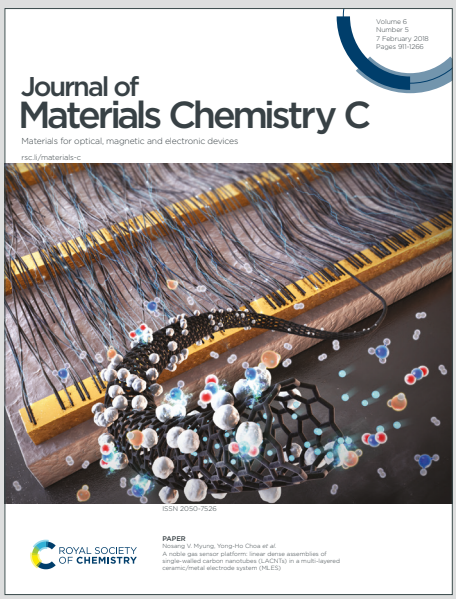




ROYAL SOCIETY OF CHEMISTRY

rsc.li/materials-c

DOI: 10.1039/D6TC00820H

# Energy Transfer Mediated Rabi Splitting in Ag@$CsPbCl_3$ Nanohybrids

Abhishek Kumar, Eeshani Bora and Tushar Debnath

Nano Physical Spectroscopy Group, Department of Chemistry, School of Natural Sciences, Shiv Nadar Institution of Eminence, Delhi NCR, Uttar Pradesh 201314, India

Email: tushar.debnath@snu.edu.in, debnathtushar@gmail.com



View Article Online
DOI: 10.1039/D6TC00820H



**Abstract**

We report a strong exciton (semiconductor) – plasmon (metal) coupling in colloidal Ag@$CsPbCl_3$ nanohybrids, leading to the emergence of new hybrid states, known as plexcitons. Here, we systematically tuned the energy separation between these hybrid states at zero-detuning energy, the so-called Rabi splitting, apparent from the simultaneous blue and red shift of the exciton and plasmon resonances, respectively. We observe an extremely large Rabi splitting from the absorption measurement, reaching a value as high as 316 meV. The plexciton energies are modelled using a dissipative coupled-oscillator framework, revealing collective coupling strengths that place the system in both the real and strong coupling regimes. We further establish an active energy transfer process between the $CsPbCl_3$ excitons and Ag plasmons, which underlies the observed strong coupling. The pronounced Rabi splitting observed in colloidal metal-semiconductor nanohybrids establishes a foundation for advancing nonlinear plasmonic technologies.

Keywords.

Perovskite nanocrystals, exciton-plasmon coupling, Rabi splitting, energy transfer, plexciton, coupled oscillator model

View Article Online
DOI: 10.1039/D6TC00820H





## Introduction.

The superposition of quantum emitters and surface plasmon polaritons greatly enhances the electromagnetic field strengths by concentrating light-matter interaction at the nanoscale.[1, 2] The coupling between these two modes leads to emergence of two distinct regimes. The interaction in the weak coupling regime partially modifies the radiative decay of the electronic excitations, while the mode frequencies are slightly altered.[3] In contrast, when the interaction between these modes is very strong, it leads to significant changes in the emission properties. In the strong coupling regime, the initial wavefunctions of the excitations and optical modes resonate with one another, allowing for coherent energy exchange. The interaction is so intense that it causes mixing and frequency repulsion between the two states, leading to the formation of two hybrid modes known as upper and lower polaritons. At zero-detuning energy, these polaritons are separated in energy by an amount called the Rabi splitting, which quantifies the strength of the light–matter interaction.[4-7]

The polarization induced due to the collective electron oscillations of metal nanostructures leads to generation of localized surface plasmonic resonances (LSPR).[8] Such plasmons behaves like an optical resonator and thus may couple with the electronic excitations (i.e. excitons).[9, 10] Strong exciton-plasmon coupling can be achieved using various organic molecules, particularly organic J-aggregates, resulting in the formation of two hybrid resonances (plexcitons), as discussed earlier.[11, 12] These plexcitonic states are separated by a large Rabi energy, which is a hallmark of the strong coupling regime.[13] Formation of plexcitons and subsequent Rabi splitting is also observed from the interaction of strong excitons from inorganic semiconductors, such as MoS2, WSe2, CdSe quantum dots (QDs) etc., and LSPR of metal nanostructures, although to a lesser extent.[14-16] In most previous studies, the detuning between exciton and plasmon resonances is varied to observe anticrossing and determine the Rabi splitting at the zero-detuning. However, the Rabi splitting energy itself is typically fixed by the intrinsic coupling strength of the system. Systematic control of the Rabi splitting at zero detuning remains relatively limited and therefore represents an important direction for engineering tunable polaritonic systems.

The high absorption cross-section and excellent photoluminescence (PL) properties of QDs make them highly attractive candidates for a wide range of optoelectronic applications, particularly in nanoplasmonic devices.[17] While halide perovskite nanocrystals (NCs) have emerged over the past decade as promising materials for energy and optoelectronic

View Article Online
DOI: 10.1039/D6TC00820H

applications,[18, 19] there is still limited literature on their coupling with plasmonic metals.[20-22] Coupling with plasmonic metals may significantly broaden the application of perovskite NCs in non-linear plasmonic devices. In our recent study, we explored the plexciton formation in plasmonic perovskite NC systems;[23] however, no Rabi splitting was observed as the detuning energy was non-zero, indicating that further detailed investigation is necessary.

In this paper, we experimentally observe a strong exciton-plasmon coupling, leading to formation of new hybrid states (i.e. plexcitons), in the colloidal Ag incorporated $CsPbCl_3$ NCs (named as Ag@CPCl nanohybrids). By playing with the Ag to $CsPbCl_3$ concentration, we systematically tuned the energy separation between the two hybrid states at zero-detuning energy, the so-called Rabi splitting. We model the observed plexciton energies using a dissipative coupled-oscillator model to quantify the exciton–plasmon coupling strength. Further, steady-state and time-resolved PL measurements were employed to investigate the underlying mechanism of the strong exciton–plasmon coupling, revealing evidence of an active energy transfer process from $CsPbCl_3$ excitons to Ag plasmons.

## Experimental.

### Materials

Cesium carbonate ($CsCO_3$, 99.9%, Spectrochem), lead bromide ($PbBr_2$, 99%, Loba Chemie), lead chloride ($PbCl_2$, ≥99.9% , Sigma –Aldrich), silver nitrate ($AgNO_3$, 99.9% , Sigma – Aldrich), oleylamine (OLA, 98%, otto chemie,), oleic Acid (OA, Sigma –Aldrich, 90%), octadecene (ODE, 90%, Thermoscientific), n- hexane (99%, Finar), ethanol (Finar). All the reagents were directly used as purchased.

### Synthesis of Ag Nanoparticles

0.17 g of silver nitrate (1 mmol) was mixed with 0.5 mL oleylamine and 4.5 mL oleic acid. The mixture was heated at 70 °C for 1.5 hours, then further heated to 180 °C at a rate of 2 °C/min. After cooling, 10 mL of toluene and 50 mL of ethanol were added to precipitate the nanoparticles. The solution was centrifuged at 8000 rpm for 10 minutes, the supernatant was discarded, and the particles were redispersed in 10 mL hexane.

### Synthesis of $CsPbCl_3$ Nanoparticles

View Article Online
DOI: 10.1039/D0TC00820H

A stock cesium oleate solution was prepared by dissolving 0.407 g $CsCO_3$ in 1.25 ml oleic acid (OA) and 20 ml ODE at 120 °C.

Separately, 0.188 mmol $PbCl_2$ was dissolved in 0.5 ml OA, 0.5 ml OLA, and 5 ml ODE at 120 °C for 30 minutes. The temperature was then raised to 165 °C, and 400 µl of the Cs-oleate solution was quickly injected, forming $CsPbCl_3$ nanocrystals. The reaction was immediately quenched in an ice water bath.

The $CsPbCl_3$ NC mixture was centrifuged at 10,000 rpm for 10 min; the supernatant was discarded. The precipitate was redispersed in 2 ml hexane and centrifuged again at 5,000 rpm for 5 min. The final supernatant was collected for further use.

**Preparation of $PbBr_2$ Precursor**

0.2 mmol of $PbBr_2$ is dissolved in a mixture of 10 mL hexane, 0.4 mL oleic acid, and 0.4 mL oleylamine by stirring at 100°C.

**Characterization**

The morphology of Ag@$CsPbCl_3$ NCs were measured using TEM and HRTEM (JEOL JEM 2100F with maximum accelerating voltage: 200KV). SHIMADZU UV-2600i UV-vis spectrophotometer was used to measure UV-vis absorption. Edinburg FS5 Fluorescence spectrophotometer was used to measure PL and time-resolved PL.

**Results and Discussions.**

CPCl NCs were synthesized by the colloidal hot injection method and stored in hexane, as reported previously.[24] Ag NPs were synthesized via ligand-assisted thermal reduction in oleylamine/oleic acid.[25] The coupled colloidal Ag@CPCl nanohybrids were prepared by mixing Ag NPs and CPCl NCs at various ratio using a vortex at 3000 rpm for one minute, as shown in Figure 1a. TEM measurement was performed to understand the morphology of the synthesized CPCl NCs. As shown in Figure 1b, cubic NCs of size ~10 – 12 nm is formed. The lattice fringes are clearly visible in the high-resolution TEM (HRTEM) images in Figure 1c, directing high crystallinity of the materials. Further, TEM characterization confirmed the successful formation of Ag@CPCl nanohybrids, as shown in Figure 1d, where the larger cubes represent CPCl NCs and the black spherical dots on the cubes correspond to Ag NPs. Additionally, HRTEM image in Figure 1e reveals a distinct darker region of ~5–6 nm

View Article Online
DOI: 10.1039/D0TC00820H

corresponding to Ag NPs, along with a clear interface between the two components. The HRTEM imaging depicts the lattice fringes, directing highly crystalline material is formed.

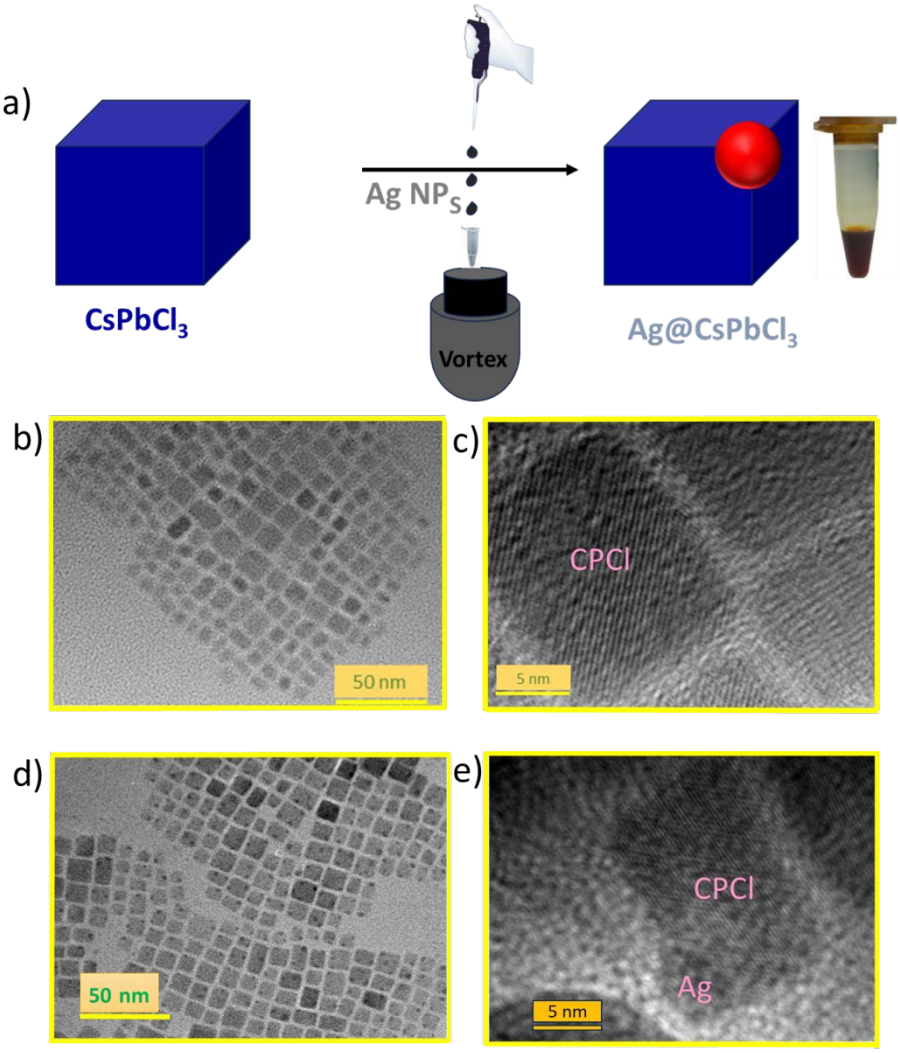


Figure 1. a) Schematic illustration of the synthesis procedure of Ag@CPCl NCs. b) TEM and c) HRTEM image of CPCl NCs. d) TEM and e) HRTEM image of Ag@CPCl NCs.

With the successful synthesis and characterization of Ag@CPCl nanohybrids, our interest is to study optical properties using UV-vis absorption, PL and time-resolved PL spectroscopy. The UV-vis optical absorption measurements reveal that the pure CPCl NCs show a sharp excitonic resonance at ~405 nm, typical for this NCs (Figure 2a). The pure Ag NPs exhibit a broad absorption resonance between 300 – 500 nm with a maximum at ~410 nm, arising from LSPR (Figure 2a). The absorption spectrum of Ag@CPCl nanohybrids exhibits characteristic features of both CPCl NCs and Ag NPs, indicating the coexistence of both components as shown in Figure S1. While the position of the exciton resonance of CPCl NCs remains unchanged,

View Article Online
DOI: 10.1039/D0TC00820H

interestingly, the LSPR peak position of the Ag NPs redshift to 443 nm, resulting in overall broadening of the absorption spectrum (Figure S1).

To understand if the shift in the plasmon peak position from 410 nm to 443 nm ($\Delta$E = 225 meV) is instant or gradual, we further varied CPCl to Ag concentration ratio during the preparation of Ag@CPCl nanohybrids that may convey important insight into the extent of exciton-to-plasmon interaction. First, we increase the Ag NPs concentration in this CPCl NCs to decrease the CPCl/Ag ratio. However, the absorption peak positions of exciton and plasmon in different Ag@CPCl nanohybrids remain unchanged, although the absorbance due to plasmon resonance gradually increases, suggesting an increase in the exciton-to-plasmon coupling. Then we increase the CPCl/Ag ratio by increasing the proportion of CPCl NCs in the fixed amount of Ag NPs (as used in Figure 2a) to prepare a series of Ag@CPCl nanohybrids, see Figure 2b. To our surprise, increasing the CPCl/Ag ratio by increasing the concentration of CPCl NCs results in splitting of the plasmon resonance into two peaks (inset Figure 2a). At low CPCl concentration of ~6.9 nM, where the exciton interaction is less, the plasmon resonance at 410 nm split into one red shifted peak at 438 nm and one blue shifted peak at 405 nm. On increasing the concentration of CPCl NCs, the red shift and blue shift of the respective peaks continues until 11.4 nM CPCl, when plasmon dominated red shifted peak settled at 443 nm and the exciton dominated blue shifted peak settled at 400 nm due to enhance the exciton-plasmon interaction enhances. No further shift in the respective peaks is observed upon further increasing CPCl/Ag ratio. It can be seen that the shift of the high energy peak (exciton dominated) to the blue region occurs to a lesser extent compared to the plasmon red shift.

The excitonic resonance gradually shifts to shorter (blue) wavelengths, whereas the plasmonic resonance shifts to longer (red) wavelengths, reflecting their opposite responses in the Ag@CPCl nanohybrids is further depicted in Figure 2c (and Figure S2) via probing the spectral evolution of excitonic and plasmonic dominated resonances. A maximum energy splitting of 316 meV is observed between the CPCl exciton and Ag plasmons at ~zero-detuning energy (i.e. at 410 nm) between the two resonances. Interestingly, the splitting decreases sharply with increasing Ag–CsPbCl3 separation, underscoring the strong distance dependence of exciton–plasmon coupling. While instantaneous plasmon shifts when Ag@CsPbCl3 forms prior to dilution as depicted in Figure 2b, a delayed (~50 min) shift is observed when Ag is added after dilution of CsPbCl3, as shown in Figure S3. We attribute this to slow diffusion and gradual reduction of separation, highlighting the critical role of interfacial chemistry in enabling close proximity and hybrid structure formation.



View Article Online
DOI: 10.1039/D0TC00820H

Figure 2d presents the observed optical properties expressed in terms of the energy diagram of Ag@CPCl nanohybrids at various CPCl/Ag ratios via increasing the CPCl NCs concentration. With increasing CPCl NCs, the excitonic energy gradually shifts toward higher energies (as shown with the blue arrow), while the plasmonic energy moves toward lower energies, as depicted with the red arrow. In effect, the energy splitting between the exciton and plasmon increases systematically, depicted with orange arrows. The opposite shifts of the excitonic and plasmonic resonances is observed in the earlier studies, revealing modification of the energy states due to formation of plexcitons via exciton-plasmon coupling through charge-transfer and local-field effects.[26] In most of the previous studies on plexcitons results when excitons from organic J-aggregates interact with the collective electron oscillations in metallic nanostructures.[12] The presence of very high coupling strength in such molecular aggregates enables efficient hybridization between exciton and plasmon resonances, which manifests as an energy splitting between the resulting hybrid states and commonly referred as Rabi splitting at zero-detuning energy. While Rabi splitting as large as 450 meV have been experimentally observed in plexcitons formed between organic molecules and plasmonic nanostructures[27], those involving inorganic semiconductors and plasmonic materials typically exhibit lower splitting, ranging from 100 to 300 meV.[16, 28] Our observations of simultaneous blue and red shift of exciton and plasmon resonance in Ag@CPCl nanohybrids at zero-detuning energy indicate existence of a strong coupling regime, evidenced by large Rabi splitting into upper and lower polaritonic states and show a strong CPCl/Ag ratio dependence (Figure 3a). The maximum splitting observed ($\Omega$ = 316 meV) in the developed plasmonic perovskite nanohybrids is thus one of the highest experimental Rabi splitting involving inorganic semiconductor NCs and plasmonic nanomaterials.



View Article Online
DOI: 10.1039/D6TC00820H



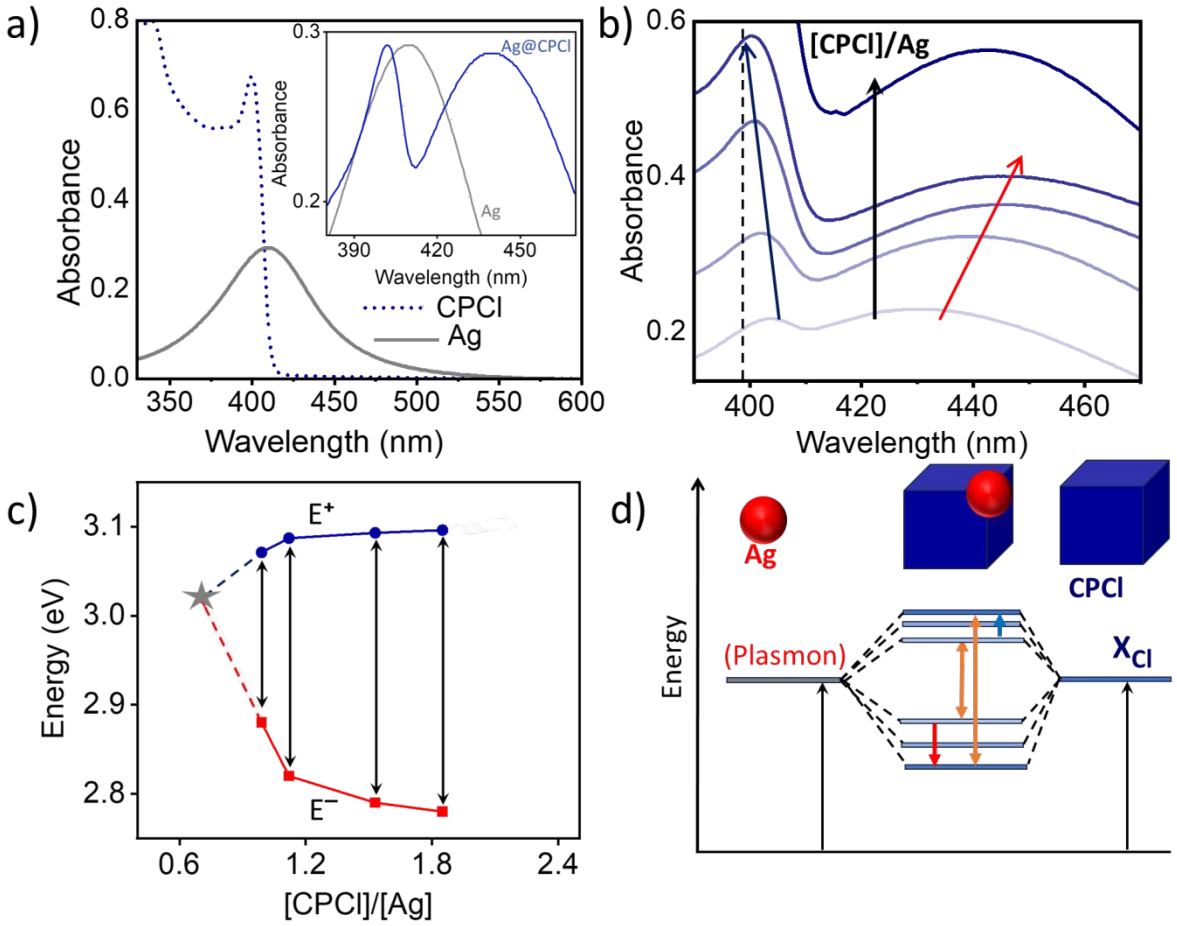


Figure 2. (a) UV–vis absorption spectra of CPCl NCs and Ag NPs. (Inset) UV–vis absorption spectrum of Ag@CPCl NCs for [CPCl] =6.9 nM and [Ag] =6.2 nM, i.e. [CPCl]/[Ag] =1.112. (b) Magnified view of the UV–vis absorption spectrum of several Ag@CPCl NCs with increasing CPCl concentration in a fixed amount of Ag NPs (i.e. varying CPCl to Ag ratio). (c) The shift in the upper ($E^+$) and lower ($E^-$) plexciton peak position as a function of CPCl to Ag concentration ratio. The symbol ★ represents the zero-detuning energy. (d) The energetics of exciton-plasmon interaction in Ag@CPCl NCs with varying CPCl to Ag ratio.

To model the observed exciton-plasmon interaction, we consider a dissipative coupled-oscillator model to describe the strong nature of the exciton–plasmon coupling in the Ag@CPCl system. The dependence of the collective exciton-plasmon coupling strength on the number of excitons were theoretically predicted by Rossi et. al. using excitonic benzene and plasmonic Al particle. [29] The collective coupling strength follows the equation:

$$g_c = \sqrt{N}\,\mu\,E_{vac} \qquad (1)$$

View Article Online
DOI: 10.1039/D6TC00820H

Here, N = effective number of excitons coupled to the plasmon mode, μ is transition dipole moment and $E_{vac}$ signifies vacuum electric field. The equation (1) immediately follows $g_c \propto \sqrt{C}$, where C is the concentration of the CPCl solution. Equation (1) further provide the single exciton (N = 1) coupling strength that can be written as $g_0 = \mu E_{vac}$. Further, the system is governed by a non-Hermitian (open) Hamiltonian operator, whose diagonal elements correspond to the damped energies of the uncoupled exciton ($E_x$) and plasmon ($E_p$) modes, while the off-diagonal elements represent the coupling strength $g_c$ between them, as shown below:

$$\hat{H} = \begin{pmatrix} E_x - \frac{i\Gamma_X}{2} & g_c \\ g_c & E_p - \frac{i\Gamma_P}{2} \end{pmatrix} = \begin{pmatrix} \tilde{E_x} & g_c \\ g_c & E_p \end{pmatrix}$$

This Hamiltonian acts on a superposition state of the plasmon and exciton modes:

$$|\psi\rangle = a|x\rangle + b|p\rangle \qquad (2)$$

The resulting hybrid eigenstates (plexcitons) are characterized by the Hopfield coefficients a and b, which quantify the excitonic and plasmonic fractions of the plexciton, respectively, and satisfy the normalization condition $|a^2| + |b^2| = 1$.[30, 31, 30] The energy of each of the coupled eigenstates (plexcitons) is then followed by solving the Schrodinger equation that can be expressed as below, where $E_+$ and $E_-$ corresponds to upper and lower plexcitons, respectively.

$$E_\pm = \frac{\tilde{E_x} + \tilde{E_p}}{2} \pm \sqrt{{g_c}^2 + \frac{(\tilde{E_x} - \tilde{E_p})^2}{4}} \qquad (3)$$

The experimental lower plexciton ($E_-$) can be best fit using the above energy expression by considering the single exciton coupling strength (normalized with respect to the added CPCl concentration) of $g_0 = 0.084 \frac{eV}{\sqrt{nM}}$. The corresponding collective coupling strength for differently added CPCl NCs concentration is shown in Figure 3b, which show an increase in the $g_c$ value with increasing CPCl concentration. Here the observed splitting scales as $\Omega_R \propto \sqrt{N}$ (Figure 3a, b) which is a signature of Rabi splitting phenomena. Using the $g_c$ values, we calculated the lower plexciton energies (theoretical) following equation (3) which matches up to the first decimal places of the experimental lower plexciton energies in all the concentration ratio, as depicted in Figure 3c. Here we probed the lower plexciton only, as the upper plexciton branch overlaps strongly with the $CsPbCl_3$ exciton resonance and thus exhibits a deviation from the coupled oscillator model, as reported previously.[31]

View Article Online
DOI: 10.1039/D0TC00820H

Now, our interest is to understand whether the observed collective coupling strength $g_c$ is real and/or strong. To this end, we need to quantify two threshold criteria. The first criteria are coming from the reduced form of the Rabi splitting which is defined as,

$$\Omega = E_+ - E_-$$

$$\Omega = 2\sqrt{{g_c}^2 - \frac{(\Gamma_P - \Gamma_X)^2}{16}} \qquad (4)$$

Equation (4) immediately follows the existence of real hybrid eigenmodes, which must satisfy the inequality,

$${g_c}^2 > \frac{(\Gamma_P - \Gamma_X)^2}{16} = A \qquad (5)$$

The second threshold criteria correspond to the strong-coupling regime, which must satisfy the following inequality,

$${g_c}^2 > \frac{(\Gamma_P + \Gamma_X)^2}{16} = B \qquad (6)$$

which means the coherent plasmon-exciton exchange rate surpasses damping rate of bare plasmon and bare exciton.[30] Figure 3d shows that the calculated collective coupling strengths for all studied sample concentrations lie above both threshold criteria, indicating that the system operates in the real and strong coupling regimes across the entire concentration range investigated and thus true plexciton behaviour. This accounts for the observation of an exceptionally large Rabi splitting of $\Omega = 316$ meV in the Ag@CPCl system.

The polaritonic nature of the splitting is further confirmed through the anti-crossing phenomenon. By tuning the CsPbX3 NCs (X = Cl, Br) bandgap, we varied the plasmon–exciton detuning and observed clear anti-crossing behaviour (Figure S4), a hallmark of polaritonic splitting.[31] Moreover, the plasmon response of Ag@CsPb(Cl:Br)3 shows negligible spectral shift relative to bare Ag nanoparticles (Figure S5), consistent with negligible exciton–plasmon overlap. As both Ag@CsPbCl3 and Ag@CsPb(Cl:Br)3 samples were prepared similarly, their dielectric environments are comparable. Therefore, the pronounced spectral shift in Ag@CsPbCl3 (Figure 2) arises from its polaritonic nature rather than changes in the local environments (such as refractive index).

View Article Online
DOI: 10.1039/D6TC00820H



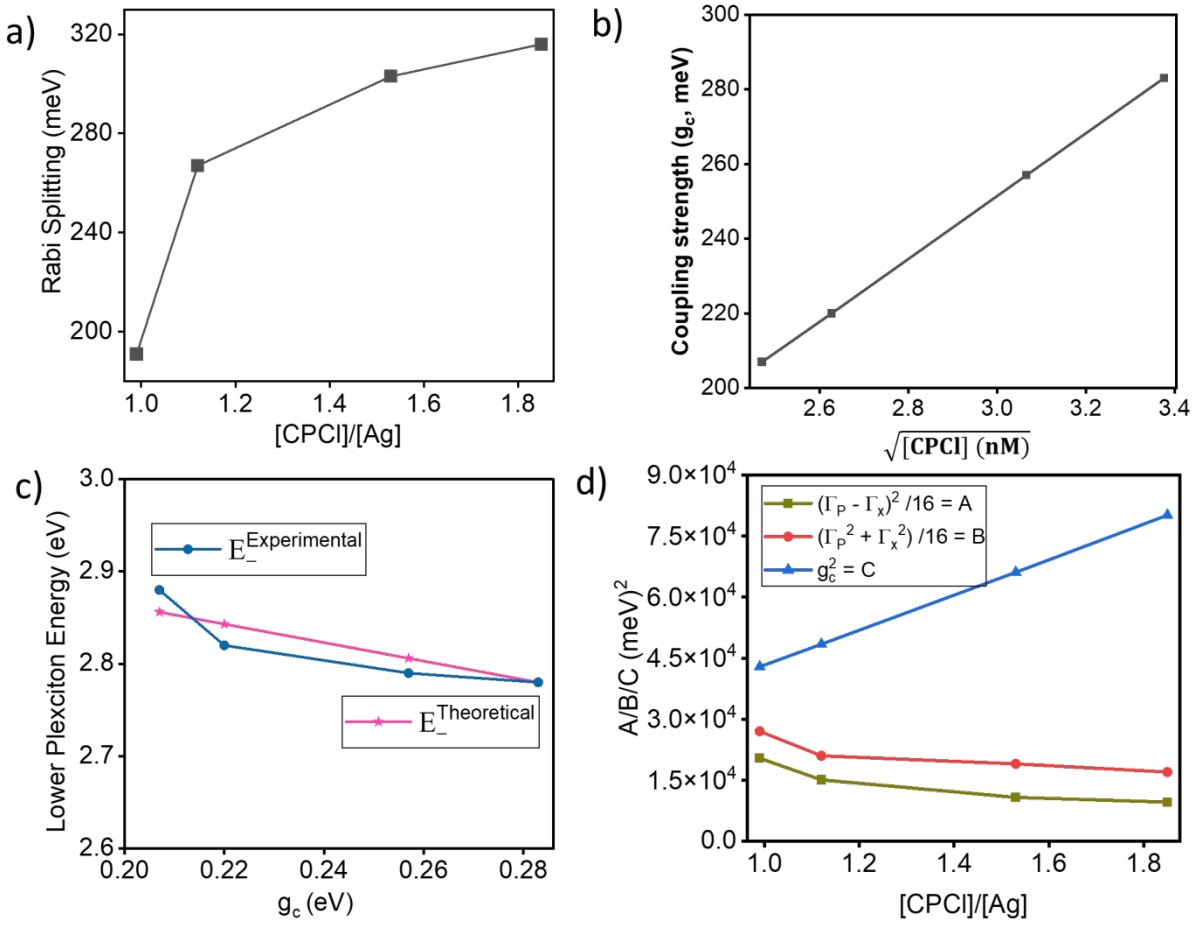


Figure 3. (a) The plot of experimental Rabi splitting (in meV) with respect to the [CPCl]/[Ag] ratio. (b) The plot of collective coherent coupling strength (in meV) with respect to the concentration CPCl NCs. (c) Comparison of the theoretical and experimental lower plexciton energies with respect to collective coupling strengths in eV. (d) Plot showing the two threshold criteria for the real and strong coupling conditions.

In order to understand the underlying mechanism of exciton-plasmon coupling in the Ag incorporated perovskite nanohybrids, we performed PL and time-resolved PL measurements of CPCl NCs in the presence of increasing Ag NPs concentration to vary CPCl/Ag ratios. The PL maximum of the pure CPCl NCs appears at 410 nm as shown in Figure 4a. Upon increasing the Ag NPs concentration so that to decrease the CPCl/Ag ratio from 1.85 to 0.99, the PL intensity of the CPCl NCs decreases gradually. A maximum of ~90 % PL quenching is observed for the CPCl/Ag ratio of 0.99. We then performed time-resolved PL decay measurement of the CPCl NCs with increasing Ag NPs concentration (Figure S6). Although

View Article Online
DOI: 10.1039/D6TC00820H

the faster lifetime component is instrument response function (IRF) limited, we observed a progressive decrease in the lifetime of the longer component with decreasing CPCl/Ag ratio. We attribute such reduction in the PL intensity and lifetime to the CPCl exciton energy transfer to Ag NPs. A strong spectral overlap (see Figure 4b) between the PL spectrum of CPCl NCs (donor) and the absorption spectrum of the Ag NPs (acceptor) allows an efficient energy transfer between the two components. This can be further evidenced by the controlled PL measurements using Ag incorporated $CsPb(Cl/Br)_3$ having different Cl/Br ratios, resulting in progressive reduction in the donor-acceptor spectral overlap (due to exciton-plasmon detuning, see Figure S7a), as shown in Figure 4b. While the Ag@CPCl nanohybrids show strongest PL quenching, as the PL of the CPCl NCs shifts in the red region via Br-exchange, the extent of PL quenching reduces gradually (Figure 4c and Figure S7b), supporting the energy transfer mechanism.

It is important to note that PL quenching may also arise from charge transfer, surface trapping which is very common in these nanocrystals. We noticed that when CsPbCl3 NCs were treated with oleyl ammonium chloride (OAmHCl), a significant PL enhancement via surface passivation occurs (Figure S8a-b).[32] However, Ag@CsPbCl3 prepared from these passivated NCs still showed pronounced PL quenching (Figure S8c), excluding surface trapping as the primary mechanism for PL quenching. Further, band alignment analysis indicates that electron transfer from photoexcited CsPbX3 (for X = Cl and Br) to Ag is thermodynamically feasible (Figure S9).[33] Nevertheless, the negligible PL quenching observed for CsPb(Cl:Br)3 in the presence of Ag suggests that charge (electron) transfer is not dominant mechanism, although a minor contribution from electron transfer cannot be neglected. The above result supports the energy transfer mechanism from the perovskite NCs to the Ag NPs as the primary underlying reason for the PL quenching, resulting in the strong plexciton formation via exciton-plasmon coupling.

View Article Online
DOI: 10.1039/D6TC00820H



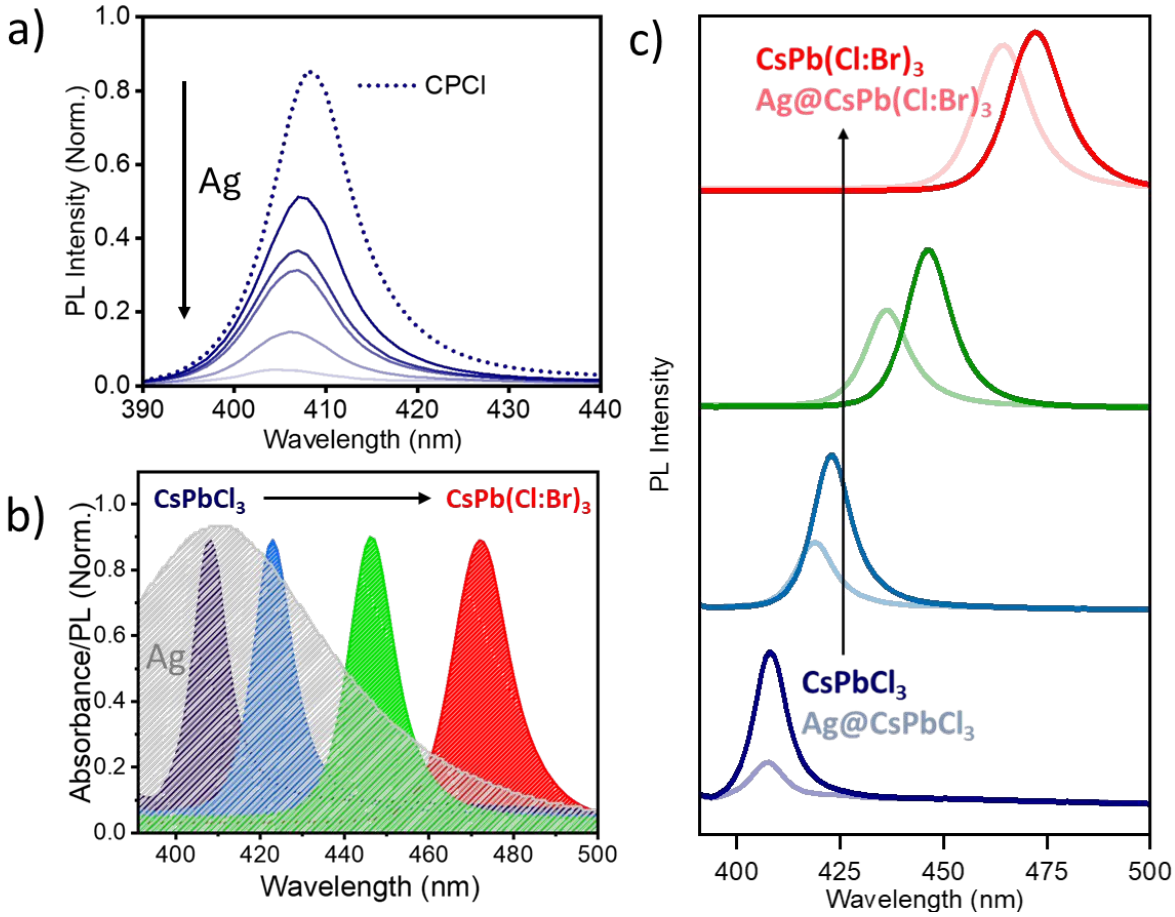


Figure 4. a) PL emission spectra of Ag@CPCl NCs with varying CPCl-to-Ag ratio. The PL spectrum of pure CPCl NCs is shown with dotted line; b) Spectral overlap between the absorption spectrum of Ag NPs and the PL emission spectra of $CsPb(Cl/Br)_3$ NCs; c) PL emission spectra of $CsPb(Cl/Br)_3$ NCs without and with Ag NPs.

**Conclusions.**

Overall, we demonstrate the existence of strong exciton-plasmon coupling in the colloidal Ag@CPCl nanohybrids, producing a new hybrid state (the plexcitons). By varying the CPCl-to-Ag ratio, we were able to systematically tune the energy separation between the two hybrid states, i.e. the Rabi splitting, reaching a value as large as 316 meV. This tuning of the Rabi splitting is evidenced by the simultaneous blue and red shifts of the exciton and plasmon resonances in the optical absorption spectra, respectively. Analysis of the plexciton energies with a dissipative coupled-oscillator model indicates that the collective coupling strengths lie within the real and strong coupling regimes. Using steady state and time-resolved PL experiments, we show energy transfer process from the CPCl exciton to Ag plasmon, causing the observation of strong exciton-plasmon coupling. The detuning of the donor-acceptor

View Article Online
DOI: 10.1039/D0TC00820H

spectral overlap via Br-exchange to produce Ag@CP(Cl/Br)$_3$ nanohybrids leads to a reduction in the PL quenching, supporting the energy transfer mechanism as the underlying reason for the efficient exciton-plasmon coupling.

Using simple optical absorption spectroscopy, we observed giant Rabi splitting by systematically controlling the system at zero detuning. The measured value represents one of the highest experimental values reported for plasmonic metal–inorganic semiconductor nanohybrids.[32] Further, the Rabi splitting follow the ideal coupled-oscillator model. This work therefore establishes a key framework for nanoplasmonic and related nonlinear applications in perovskite systems.

## Supporting information

Details about calculations, further data on absorption, PL, and lifetime analysis, etc.

## Acknowledgments

T.D. acknowledges the Department of Science & Technology (DST) and the Science and Engineering Research Board (SERB) for the Ramanujan Fellowship Award (RJF/2021/000125) and the Core Research Grant (CRG/2023/000519). E.B. thank the Science and Engineering Research Board (SERB) (project no. RJF/2021/000125) for fellowship. We thank School of Natural Sciences, Shiv Nadar Institution of Eminence for instrument support.

## Conflicts of interest

The authors declare no conflict of interest.

## References

1. Achermann, M., Exciton−Plasmon Interactions in Metal−Semiconductor Nanostructures. *The Journal of Physical Chemistry Letters* **2010,** *1* (19), 2837-2843.
2. Okamoto, K.; Niki, I.; Shvartser, A.; Narukawa, Y.; Mukai, T.; Scherer, A., Surface-plasmon-enhanced light emitters based on InGaN quantum wells. *Nature Materials* **2004,** *3* (9), 601-605.
3. Kleppner, D., Inhibited Spontaneous Emission. *Physical Review Letters* **1981,** *47* (4), 233-236.
4. Lidzey, D. G.; Bradley, D. D. C.; Skolnick, M. S.; Virgili, T.; Walker, S.; Whittaker, D. M., Strong exciton–photon coupling in an organic semiconductor microcavity. *Nature* **1998,** *395* (6697), 53-55.

View Article Online
DOI: 10.1039/D6TC00820H



5. Weisbuch, C.; Nishioka, M.; Ishikawa, A.; Arakawa, Y., Observation of the coupled exciton-photon mode splitting in a semiconductor quantum microcavity. *Physical Review Letters* **1992,** *69* (23), 3314-3317.
6. Schlather, A. E.; Large, N.; Urban, A. S.; Nordlander, P.; Halas, N. J., Near-Field Mediated Plexcitonic Coupling and Giant Rabi Splitting in Individual Metallic Dimers. *Nano Lett* **2013,** *13* (7), 3281-3286.
7. Dey, J.; Virdi, A.; Chandra, M., Plasmon–Exciton Interaction at the Nanoscale: Silver Is More "Precious" than Gold! *The Journal of Physical Chemistry Letters* **2024,** *15* (30), 7674-7680.
8. Barnes, W. L.; Dereux, A.; Ebbesen, T. W., Surface plasmon subwavelength optics. *Nature* **2003,** *424* (6950), 824-830.
9. Jain, P. K.; Eustis, S.; El-Sayed, M. A., Plasmon Coupling in Nanorod Assemblies: Optical Absorption, Discrete Dipole Approximation Simulation, and Exciton-Coupling Model. *The Journal of Physical Chemistry B* **2006,** *110* (37), 18243-18253.
10. Prodan, E.; Radloff, C.; Halas, N. J.; Nordlander, P., A Hybridization Model for the Plasmon Response of Complex Nanostructures. *Science* **2003,** *302* (5644), 419-422.
11. Manuel, A. P.; Kirkey, A.; Mahdi, N.; Shankar, K., Plexcitonics – fundamental principles and optoelectronic applications. *Journal of Materials Chemistry C* **2019,** *7* (7), 1821-1853.
12. Fofang, N. T.; Park, T.-H.; Neumann, O.; Mirin, N. A.; Nordlander, P.; Halas, N. J., Plexcitonic Nanoparticles: Plasmon−Exciton Coupling in Nanoshell−J-Aggregate Complexes. *Nano Lett* **2008,** *8* (10), 3481-3487.
13. Vasa, P.; Wang, W.; Pomraenke, R.; Lammers, M.; Maiuri, M.; Manzoni, C.; Cerullo, G.; Lienau, C., Real-time observation of ultrafast Rabi oscillations between excitons and plasmons in metal nanostructures with J-aggregates. *Nature Photonics* **2013,** *7* (2), 128-132.
14. Liu, W.; Lee, B.; Naylor, C. H.; Ee, H.-S.; Park, J.; Johnson, A. T. C.; Agarwal, R., Strong Exciton–Plasmon Coupling in MoS2 Coupled with Plasmonic Lattice. *Nano Lett* **2016,** *16* (2), 1262-1269.
15. Wang, M.; Krasnok, A.; Zhang, T.; Scarabelli, L.; Liu, H.; Wu, Z.; Liz-Marzán, L. M.; Terrones, M.; Alù, A.; Zheng, Y., Tunable Fano Resonance and Plasmon–Exciton Coupling in Single Au Nanotriangles on Monolayer WS2 at Room Temperature. *Advanced Materials* **2018,** *30* (22), 1705779.
16. Wang, H.; Wang, H.-Y.; Toma, A.; Yano, T.-a.; Chen, Q.-D.; Xu, H.-L.; Sun, H.-B.; Proietti Zaccaria, R., Dynamics of Strong Coupling between CdSe Quantum Dots and Surface Plasmon Polaritons in Subwavelength Hole Array. *The Journal of Physical Chemistry Letters* **2016,** *7* (22), 4648-4654.
17. Arquer, F. P. G. d.; Talapin, D. V.; Klimov, V. I.; Arakawa, Y.; Bayer, M.; Sargent, E. H., Semiconductor quantum dots: Technological progress and future challenges. *Science* **2021,** *373* (6555), eaaz8541.
18. Dey, A.; Ye, J.; De, A.; Debroye, E.; Ha, S. K.; Bladt, E.; Kshirsagar, A. S.; Wang, Z.; Yin, J.; Wang, Y.; Quan, L. N.; Yan, F.; Gao, M.; Li, X.; Shamsi, J.; Debnath, T.; Cao, M.; Scheel, M. A.; Kumar, S.; Steele, J. A.; Gerhard, M.; Chouhan, L.; Xu, K.; Wu, X.-g.; Li, Y.; Zhang, Y.; Dutta, A.; Han, C.; Vincon, I.; Rogach, A. L.; Nag, A.; Samanta, A.; Korgel, B. A.; Shih, C.-J.; Gamelin, D. R.; Son, D. H.; Zeng, H.; Zhong, H.; Sun, H.; Demir, H. V.; Scheblykin, I. G.; Mora-Seró, I.; Stolarczyk, J. K.; Zhang, J. Z.; Feldmann, J.; Hofkens, J.; Luther, J. M.; Pérez-Prieto, J.; Li, L.; Manna, L.; Bodnarchuk, M. I.; Kovalenko, M. V.; Roeffaers, M. B. J.; Pradhan, N.; Mohammed, O. F.; Bakr, O. M.; Yang, P.; Müller-Buschbaum, P.; Kamat, P. V.; Bao, Q.; Zhang, Q.; Krahne, R.; Galian, R. E.; Stranks, S. D.; Bals, S.; Biju, V.; Tisdale, W. A.; Yan, Y.; Hoye, R. L. Z.; Polavarapu, L., State of the Art and Prospects for Halide Perovskite Nanocrystals. *ACS Nano* **2021,** *15* (7), 10775-10981.
19. Shamsi, J.; Urban, A. S.; Imran, M.; De Trizio, L.; Manna, L., Metal Halide Perovskite Nanocrystals: Synthesis, Post-Synthesis Modifications, and Their Optical Properties. *Chemical Reviews* **2019,** *119* (5), 3296-3348.

View Article Online
DOI: 10.1039/D6TC00820H

20. Balakrishnan, S. K.; Kamat, P. V., Au–CsPbBr3 Hybrid Architecture: Anchoring Gold Nanoparticles on Cubic Perovskite Nanocrystals. *Acs Energy Lett* **2017,** *2* (1), 88-93.
21. Chen, S.; Lyu, D.; Ling, T.; Guo, W., Reversible modulation of CsPbBr3 perovskite nanocrystal/gold nanoparticle heterostructures. *Chemical Communications* **2018,** *54* (36), 4605-4608.
22. Samanta, S.; Paul, S.; Debnath, T., Obtaining Ligand-Free Aqueous Au-Nanoparticles Using Reversible CsPbBr3 ↔ Au@CsPbBr3 Nanocrystal Transformation. *Small* **2024,** *20* (19), 2311712.
23. Bora, E.; Das, J. P.; Samanta, S.; Kumar, A.; Debnath, T., Plexciton Dynamics in Au-Hybrid CsPbBr3 Perovskite Nanoplatelets. *The Journal of Physical Chemistry Letters* **2025,** *16* (28), 7134-7139.
24. Otero-Martínez, C.; García-Lojo, D.; Pastoriza-Santos, I.; Pérez-Juste, J.; Polavarapu, L., Dimensionality Control of Inorganic and Hybrid Perovskite Nanocrystals by Reaction Temperature: From No-Confinement to 3D and 1D Quantum Confinement. *Angewandte Chemie International Edition* **2021,** *60* (51), 26677-26684.
25. Park, J.; Kwon, S. G.; Jun, S. W.; Kim, B. H.; Hyeon, T., Large-Scale Synthesis of Ultra-Small-Sized Silver Nanoparticles. *ChemPhysChem* **2012,** *13* (10), 2540-2543.
26. Shahbazyan, T. V., Exciton–Plasmon Energy Exchange Drives the Transition to a Strong Coupling Regime. *Nano Lett* **2019,** *19* (5), 3273-3279.
27. Bellessa, J.; Symonds, C.; Vynck, K.; Lemaitre, A.; Brioude, A.; Beaur, L.; Plenet, J. C.; Viste, P.; Felbacq, D.; Cambril, E.; Valvin, P., Giant Rabi splitting between localized mixed plasmon-exciton states in a two-dimensional array of nanosize metallic disks in an organic semiconductor. *Phys Rev B* **2009,** *80* (3), 033303.
28. Gómez, D. E.; Vernon, K. C.; Mulvaney, P.; Davis, T. J., Surface Plasmon Mediated Strong Exciton−Photon Coupling in Semiconductor Nanocrystals. *Nano Lett* **2010,** *10* (1), 274-278.
29. Rossi, T. P.; Shegai, T.; Erhart, P.; Antosiewicz, T. J., Strong plasmon-molecule coupling at the nanoscale revealed by first-principles modeling. *Nature Communications* **2019,** *10* (1), 3336.
30. Roller, E.-M.; Argyropoulos, C.; Högele, A.; Liedl, T.; Pilo-Pais, M., Plasmon–Exciton Coupling Using DNA Templates. *Nano Lett* **2016,** *16* (9), 5962-5966.
31. Beane, G.; Brown, B. S.; Johns, P.; Devkota, T.; Hartland, G. V., Strong Exciton–Plasmon Coupling in Silver Nanowire Nanocavities. *The Journal of Physical Chemistry Letters* **2018,** *9* (7), 1676-1681.
32. Shah, S. H.; Debnath, T., CuInS2-Decorated Perovskite Nanoarchitecture: Halide-Driven Energy and Electron Transfer. *The Journal of Physical Chemistry Letters* **2024,** *15* (9), 2580-2586.
33. Huang, X.; Li, H.; Zhang, C.; Tan, S.; Chen, Z.; Chen, L.; Lu, Z.; Wang, X.; Xiao, M., Efficient plasmon-hot electron conversion in Ag–CsPbBr3 hybrid nanocrystals. *Nature Communications* **2019,** *10* (1), 1163.

View Article Online
DOI: 10.1039/D6TC00820H

Data Availability Statement:

Data is available from the corresponding author upon reasonable request.